CORE
Metadata, citation and similar papers at core.ac.uk
Provided by IntechOpen

We are IntechOpen,
the world's leading publisher of
Open Access books
Built by scientists, for scientists

4,800
Open access books available

122,000
International authors and editors

135M
Downloads

154
Countries delivered to

Our authors are among the
TOP 1%
most cited scientists

12.2%
Contributors from top 500 universities

WEB OF SCIENCE™
Selection of our books indexed in the Book Citation Index
in Web of Science™ Core Collection (BKCI)

Interested in publishing with us?
Contact book.department@intechopen.com

Numbers displayed above are based on latest data collected.
For more information visit www.intechopen.com

14

A Pearson Effective Potential for Monte-Carlo Simulation of Quantum Confinement Effects in nMOSFETs

Marie-Anne Jaud[1], Sylvain Barraud[1], Philippe Dollfus[2], Jérôme Saint-Martin[2], Arnaud Bournel[2] and Hervé Jaouen[3]

[1]*CEA-LETI, MINATEC, 17 rue des Martyrs, 38054 Grenoble,*
[2]*Institut d'Electronique Fondamentale, CNRS UMR 8622, Bât. 220, Univ. Paris-Sud, 91405 Orsay,*
[3]*STMicroelectronics, 850 rue Jean Monnet, 38926 Crolles, France*

1. Introduction

As MOSFETs are downscaled to nanometric dimensions, ultra-thin body devices are required for an optimal electrostatic channel control. In such devices, quantization effects are likely to have a large impact on both electrostatics and carrier transport properties. Consequently, to accurately investigate electron transport in ultimate MOSFET architectures, the usual semi-classical transport models can no longer be applied and new simulation tools accounting for quantum effects in the electron transport description are becoming of great relevance.

In the last few years, some works investigated the possibility to develop quantum models based on a particle description of transport. Given the strong analogy between Wigner and Boltzmann formalisms, the Monte-Carlo method commonly used for semi-classical transport simulation can be extended to the quantum case by considering the Wigner function as an ensemble of pseudo-particles (Shifren et al., 2003 ; Nedjalkov et al., 2004 ; Querlioz et al., 2006). This approach describes well the wave-like nature of particles and has been first applied to the one-dimensional (1D) simulation of double-barrier resonant structures. To treat quantization effects in an inversion channel, one may couple self-consistently the 1D Schrödinger equation solved along the confinement direction with the multi-subband Boltzmann transport in the source-to-drain direction including 2D scattering rates (Lucci et al., 2005 ; Saint-Martin et al., 2006). This mode-space approach properly accounts for quantization effects in ultra-thin double-gate devices but is computationally intensive and may be difficult to extend to other architectures. Recently, some works combining the two previous methods for studying quantum transport in ultra-scaled double-gate MOSFETs have been published (Sverdlov et al., 2005; Querlioz et al., 2007). Alternatives to the mode-space approach are the quantum corrected potential methods (Ferry et al., 2000; Akis et al., 2001; Li et al., 2002; Tang et al., 2003; Tsuchiya et al., 2003; Fan et al., 2004; Ahmed et al., 2005; Riolino et al., 2006; Jaud et al., 2006) which have been demonstrated as an efficient way for including quantization effects in a semi-classical

particle Monte-Carlo simulator. Among these techniques, the Gaussian Effective Potential (GEP) formulation (Ferry et al., 2000; Akis et al., 2001; Li et al., 2002; Palestri et al., 2005; Jaud et al., 2006) is of great interest because it is weakly sensitive to the particle noise inherent in Monte-Carlo simulation and it is an alternative to the Schrödinger-Poisson based effective potential (Fan et al., 2004) that requires to solving the Schrödinger's equation. As already reported in (Li et al., 2002; Palestri et al., 2005; Jaud et al., 2006), the GEP correction can accurately reproduce Schrödinger-Poisson (SP) integral quantities such as the total inversion charge but fails to correctly model the electron density profiles. The discrepancy between GEP and SP density profiles is particularly important close to the SiO_2/Si interfaces. It is thus especially critical in ultra-thin double-gate structures where electron wave functions are affected by two such interfaces.

In this chapter, we demonstrate the ability of an original Effective Potential formalism to properly introduce the quantum confinement effects in a Monte-Carlo simulator, i.e. not only the electrostatics in long nMOS capacitors but also the electron transport in nanoscale nMOSFET devices. In section 2, we briefly outline the quantum corrected potential approach for Monte-Carlo simulation. Section 3 highlights and investigates the limitations of the usual Gaussian Effective Potential (GEP). This leads us to develop a novel Pearson Effective Potential (PEP) correction, whose detailed description, electrostatic validation on various MOS architectures and extension to source and drain areas are described in sections 4, 5 and 6, respectively. Section 7 compares the results obtained from semi-classical, GEP corrected, PEP corrected and multi-subband Monte-Carlo methods for an ultra-short double-gate nMOSFET at low and high drain voltage. Finally, the influence of quantum confinement effects on the drive current as a function of both the channel length and the silicon film thickness is discussed in section 8.

2. Quantum corrected potential approach

The quantum corrected potential concept has been first introduced by Madelung and Bohm (Madelung, 1926; Bohm, 1952). Its aim is to reproduce physical effects due to quantization by modifying the electrostatic potential responsible for the carrier movement. The flowchart of the quantum corrected Monte-Carlo algorithm together with an illustration of the potential and of the electron density as a function of the distance from an oxide/silicon interface along the confinement direction (referred to as x-axis) are presented in Fig. 1.

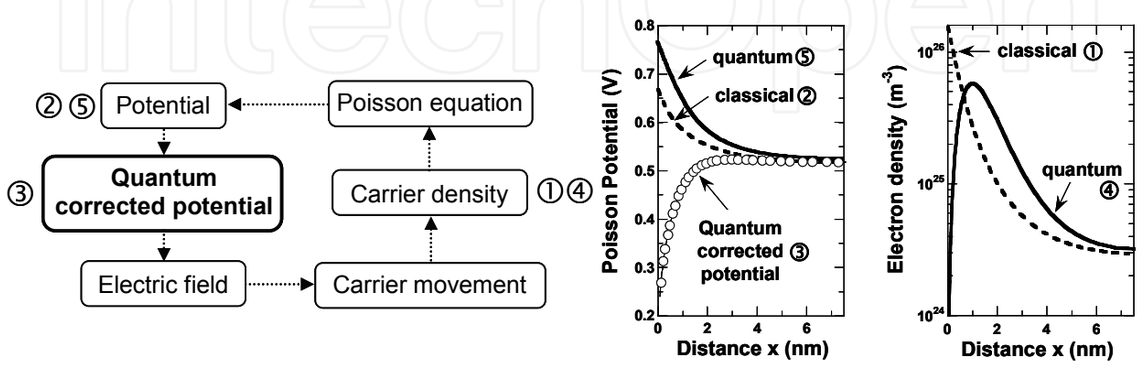

Fig. 1. Principle of the quantum corrected Monte Carlo simulation.

At first, the potential obtained from Poisson's equation solution is used to calculate the quantum corrected potential to be introduced in the Monte-Carlo algorithm for the calculation of carrier trajectories. The resulting quantum corrected potential generates an electric field that tends to repel carriers from the oxide/silicon interfaces in accordance with quantization effects. The carrier repulsion at interface is thus naturally included in the standard Monte-Carlo algorithm. As expected, the Poisson equation solution leads to a "quantum" potential which has a higher curvature than the "classical" potential. Finally, the self-consistency between quantum corrected potential and carrier movement is obtained from an iterative procedure. Within this approach, only the free-flight carrier trajectories are modified by the quantum correction. Scattering mechanisms are assumed to be identical to those of a conventional semi-classical Monte-Carlo approach.

3. Gaussian effective potential model

3.1 Theoretical model

The effective potential formalism has been originally developed by Feynman (Feynman & Hibbs, 1965). It accounts for carrier non-locality by considering the finite size of the carrier wave-packet. As a result, a carrier is not only influenced by the local potential at its position but also by the neighboring potential distribution. The usual Gaussian Effective Potential (GEP) is defined along the confinement direction by the convolution of the Poisson potential with a Gaussian function representing the electron wave-packet (Feynman & Hibbs, 1965; Ferry et al., 2000):

$$\mathrm{GEP}(x) = \frac{1}{\sqrt{2\pi}\,\sigma_x} \int_{-T_{ox}}^{T_{Si}+T_{ox}} V_P(x') \times \exp\left(-\frac{|x-x'|^2}{2\sigma_x^2}\right) dx' \tag{1}$$

where σ_x is the standard deviation of the Gaussian function, T_{Si} the silicon film thickness, T_{ox} the oxide thickness and $V_P(x')$ the Poisson potential. As explained in (Jaud et al., 2006), the GEP is calculated using a Fourier transform method. Accordingly, to apply appropriate boundary conditions to the Poisson potential on the oxide areas and to avoid data corruption by convolution in equation (1), *"Padding regions"* (by reference to signal processing techniques) are used on the edge of the device. The parameter $E_B = 3.1$ eV is defined at the SiO_2/Si interfaces to represent the oxide barrier height for electrons and satisfies $V_{oxide} = V_P - E_B$.

3.2 Results and discussion

As described in (Jaud et al., 2006), we have implemented the GEP correction in the framework of a Monte-Carlo code (MONACO) (Saint-Martin et al., 2004) that uses an analytical conduction-band structure of silicon considering six ellipsoidal nonparabolic Δ valleys. Double-gate nMOS capacitors with a channel doping $N_A = 10^{16}$ cm^{-3} and an oxide thickness $T_{ox} = 1$ nm have been simulated. Self-consistent Monte-Carlo simulations corrected by the GEP have been performed for a large range of silicon thicknesses (5 nm $\leq T_{Si} \leq$ 20 nm) together with a perpendicular effective field E_{eff} varying from 10^5 V.cm^{-1} to 10^6 V.cm^{-1}. In accordance with (Akis et al., 2001; Palestri et al., 2005), the standard deviation of the Gaussian function is chosen to be equal to $\sigma_x = 0.5$ nm. Considering the results from SP simulations including the 2-fold and 4-fold valleys with 10 energy levels for each valley as reference, Fig. 2a shows the error on the inversion charge induced by the GEP correction.

Fig. 2b compares the electron density resulting from the GEP correction with the one resulting from SP simulation for T_{Si} = 10 nm. The GEP formalism is well-known and has been proved to be useful to describe "electrostatic quantum effects" (Ferry et al., 2000 ; Akis et al., 2001 ; Li et al., 2002 ; Palestri et al., 2005). However, errors higher than 10% on the inversion charge are observed at $E_{eff} = 10^5$ V.cm^{-1}. At this low effective field, a decrease of the silicon thickness yields a noticeable increase of the inversion charge error (cf. Fig. 2a). Moreover, in agreement with (Li et al., 2002 ; Palestri et al., 2005), one can observe in Fig. 2b that the results obtained from Monte-Carlo simulation corrected by the GEP show an overestimated carrier repulsion at the SiO_2/Si interfaces. This is due to the fact that the electron wave-packet is systematically represented by an unique Gaussian function, defined by a standard deviation σ_x and an average position R_p, all along the silicon film thickness. Close to the SiO_2/Si interfaces, this description is not realistic with regard to SP results. The inability of the Gaussian function to represent the electron wave-packet has been clearly highlighted in (Jaud et al., 2006) using a methodology based on a design-of-experiments. It has been proved impossible to find out any values of E_B and σ_x likely to properly reproduce the SP carrier density profile.

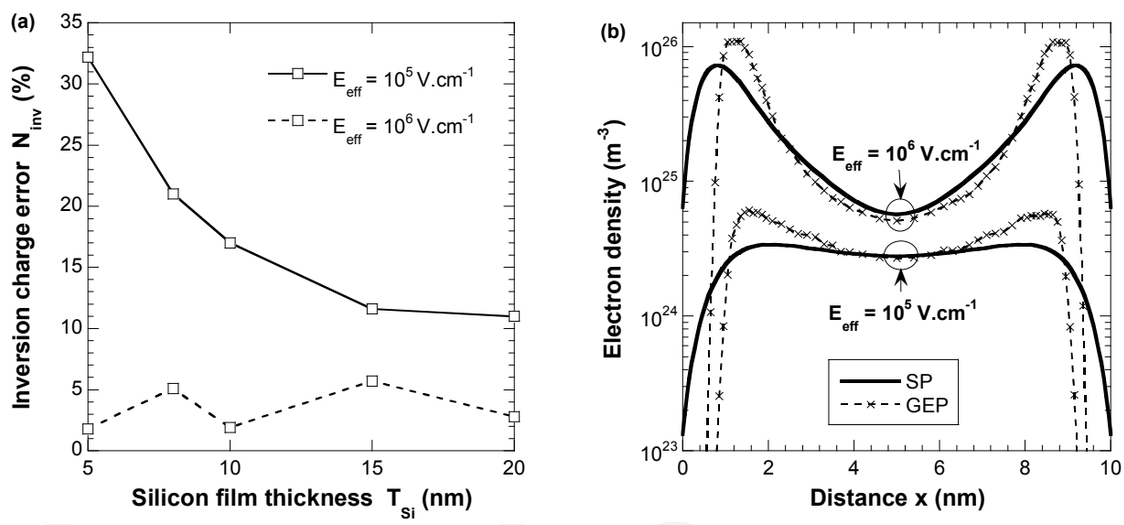

Fig. 2. (a) Inversion charge error in GEP correction (with standard parameters E_B = 3.1 eV and σ_x = 0.5 nm) as a function of the silicon film thickness of double-gate nMOS capacitors for 10^5 V.cm^{-1} (solid line) and 10^6 V.cm^{-1} (dotted line) perpendicular effective fields.
(b) Electron density as a function of the distance in the confinement direction in a double-gate nMOS capacitor with T_{Si} = 10 nm using Schrödinger-Poisson (SP - solid lines) and Monte-Carlo corrected by the GEP (GEP – cross dotted lines) models.

4. Pearson effective potential model

4.1 General principle

The previous study based on the GEP correction leads us to propose a new Effective Potential formalism where the electron wave-packet description is improved. The Gaussian function is replaced by a more realistic function based on the shape of the squared modulus of the first level Schrödinger's wave function $|\psi_0|^2$ and carefully calibrated so as to reproduce the electron density profiles resulting from SP simulations considering 10 energy

levels. Before calibrating our new function, we first have (i) to choose a well-suited function to reproduce the different possible shapes of $|\psi_0|^2$; (ii) to identify the parameters responsible for the main characteristics of the shape of $|\psi_0|^2$, i.e., to determine the dependences to be given to the new electron wave-packet description. This will lead us to define our novel effective potential formulation.

Electron wave-packet's description

To well describe the various shapes of $|\psi_0|^2$, the new function has to verify the two following conditions: (i) to be a generalization of the Gaussian distribution and (ii) to be possibly asymmetrical. The *Pearson type IV distribution*, often used for the description of doping implantation profiles, fully satisfies these conditions. It is defined by its first four moments which are related to the average position (R_p), the standard deviation (σ_p), the skewness (γ) and the kurtosis (β) of the distribution, respectively (Selberherr, 1984; Sze, 1988) (see 11. Appendix). Fig. 3 illustrates the influence of each Pearson IV parameter. The skewness and the kurtosis are a measure of the *asymmetry* and *peakedness* of the distribution function, respectively. A positive, respectively negative, value of the skewness results in a maximum of the distribution on the left, respectively on the right, of its average position (cf. Fig. 3b). We can note that a Gaussian function is a particular Pearson IV distribution defined by $\gamma = 0$ and $\beta = 3$.

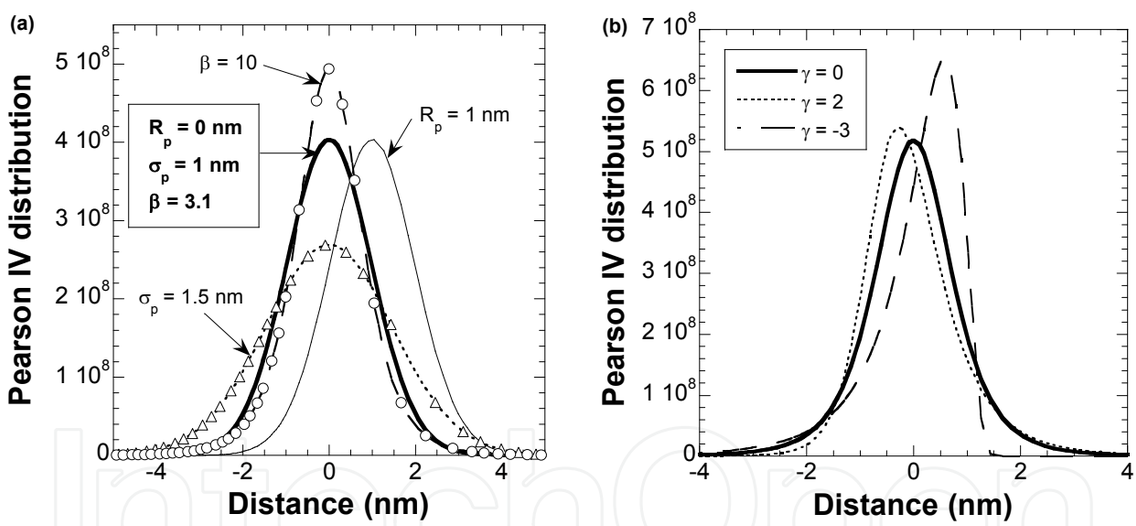

Fig. 3. Pearson IV distributions. (a) $R_p = 0$ nm, $\sigma_p = 1$ nm, $\gamma = 0$, $\beta = 3.1$ (solid heavy line) / $R_p = 1$ nm, $\sigma_p = 1$ nm, $\gamma = 0$, $\beta = 3.1$ (solid line) / $R_p = 0$ nm, $\sigma_p = 1.5$ nm, $\gamma = 0$, $\beta = 3.1$ (open triangles) / $R_p = 0$ nm, $\sigma_p = 1$ nm, $\gamma = 0$, $\beta = 10$ (open circles). (b) $R_p = 0$ nm, $\sigma_p = 1$ nm, $\beta = 30$.

Electron wave-packet's dependences

It is well-known that the shape of $|\psi_0|^2$ is primarily influenced (i) by the potential profile in the confinement direction and (ii) by the silicon film thickness. Therefore, so as to realistically describe the particle wave-packet, Pearson IV parameters should depend (i) on the local electric field E_x in the confinement direction, calculated as the derivative of the potential obtained from Poisson's equation in the confinement direction and (ii) on the silicon film thickness T_{Si}. This way, the influence of parameters such as T_{ox}, N_A or gate voltage is implicitly taken into account through the E_x-dependence.

Pearson Effective Potential formulation

As in the GEP approach, our PEP formulation is based on the convolution of the Poisson potential by a Pearson IV function representing the non zero-size of the electron wave-packet (Feynman & Hibbs, 1965; Ferry et al., 2000). For a double-gate structure it is defined (1D) as:

$$\mathrm{PEP}(x) = \int_{-T_{ox}}^{T_{Si}+T_{ox}} \left[V_P(x') * \text{Pearson IV } (R_p(E_x, T_{Si}) - x') \right] dx' \tag{2}$$

where $V_P(x')$ is the potential energy, T_{Si} and T_{ox} are the silicon film and oxide thicknesses, and E_x is the local electric field in the confinement direction.

4.2 Calibration

To calibrate the four moments of the Pearson IV distribution, the Schrödinger-Poisson equations considering 10 energy levels have been solved self-consistently for double-gate nMOS capacitors with silicon film thickness varying from 5 nm ≤ T_{Si} ≤ 20 nm and for a large range of effective fields (10^5 V.cm^{-1} ≤ E_{eff} ≤ 10^6 V.cm^{-1}). Indeed, double-gate capacitors with T_{Si} less than 5 nm are not very realistic for actual technological purposes and the chosen range of effective fields is similar to the values used for the effective mobility extraction in the inversion layer of long-channel devices.

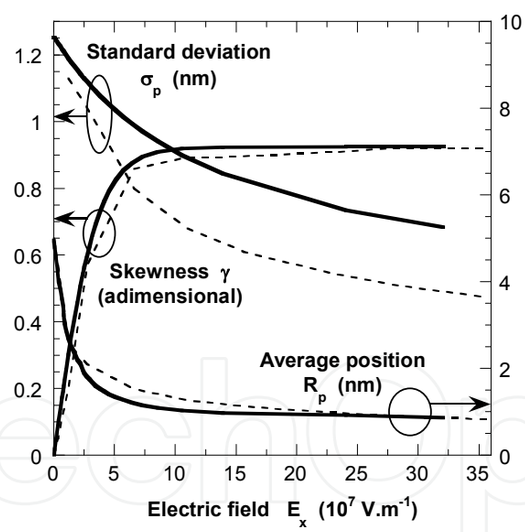

Fig. 4. R_p, σ_p and γ as a function of the electric field E_x in the confinement direction extracted from the squared modulus of the first level Schrödinger's wave function (dotted lines) and defining the Pearson IV distribution of the PEP model (solid lines) for T_{Si} = 10 nm.

For each device and effective field, the interfacial electric field, the squared modulus of the first level Schrödinger's wave function $|\psi_0|^2$ and the electron density profile have been extracted. Then, each of the first four theoretical moments of $|\psi_0|^2$ has been calculated as a function of the interfacial electric field and of the silicon film thickness. Thereafter, the terminology "theoretical values" refers to these moment values deduced from SP $|\psi_0|^2$ functions. In the case of a 10 nm film thickness double-gate capacitor, the theoretical values

of the average position with respect to the oxide-silicon interface, the standard deviation and the skewness are plotted in dotted lines as a function of the interfacial electric field on Fig. 4. When decreasing the electric field, the average position is farther away from oxide/silicon interface, the standard deviation is greater and the skewness is smaller, which is in accordance with less pronounced quantum confinement effects. The first four moments defining the Pearson IV distributions were calibrated using appropriate functions both to fit theoretical values of $|\psi_0|^2$ as closely as possible and to reproduce SP electron density profiles. The solid lines of Fig. 4 shows the calibration results of average position, standard deviation and skewness obtained for a double-gate capacitor of 10 nm film thickness. Moreover, for this structure in inversion regime, some Pearson IV distributions associated with various carrier positions in the silicon film as well as the first four moments of the Pearson IV are plotted on Fig. 5 along the confinement direction.

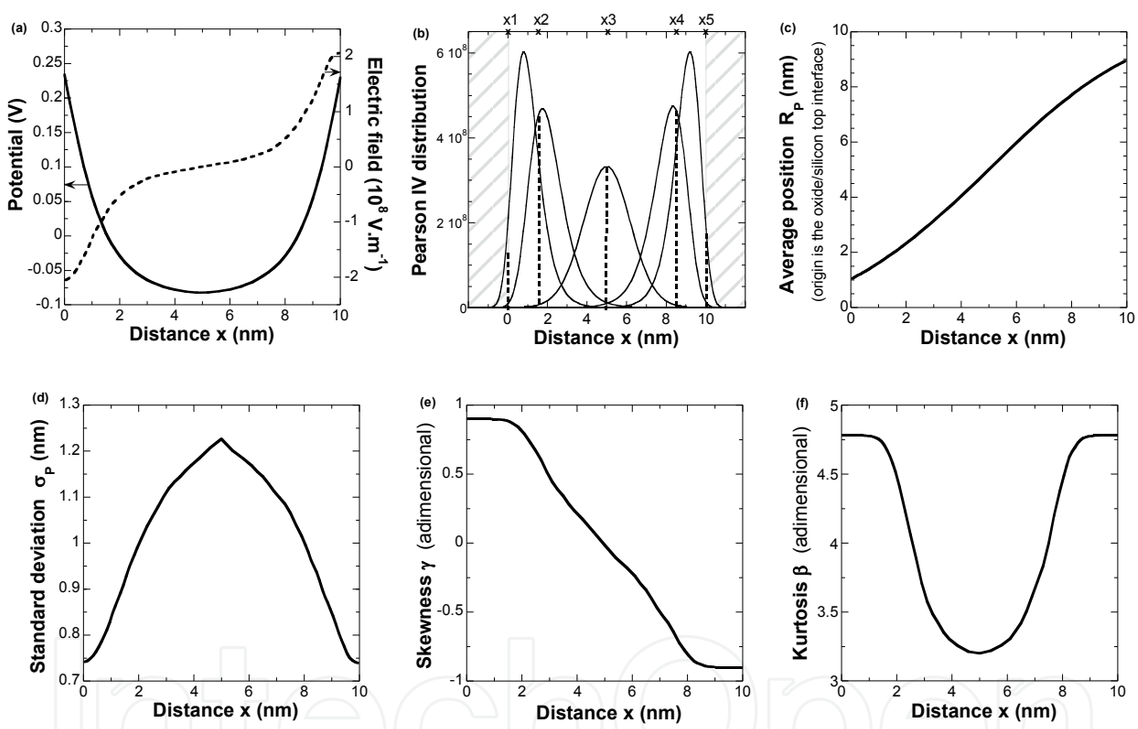

Fig. 5. Poisson potential and local electric field (a), Pearson IV distributions representing the electron wave-packets associated to various electron positions (symbolized by dotted lines) (b), R_p (c), σ_p (d), γ (e) and β (f) as a function of the distance along the confinement direction for a T_{Si} = 10 nm double-gate nMOS capacitor in inversion regime.

Now we describe in more details the fitting procedure. The expressions of Pearson IV moments as a function of E_x and T_{Si} together with the resulting fitting parameters are given in (11. Appendix).

- For the definition of the average position (R_p), the position of the oxide/silicon top interface is taken as reference. As a function of E_x and T_{Si}, R_p is chosen to fit the theoretical values (cf. Fig. 4) while ensuring that (i) in the case of a zero electric field the average position R_p is equal to the particle position and (ii) the R_p evolution along the

confinement direction x is continuous and regular, a necessary condition for the numerical stability of the algorithm. We can note in Fig. 5c that the average position of the wave-packet of a particle located at the oxide/silicon interface is at about 1 nm apart from this interface, which prevents from unrealistic wave-packet penetration in the oxide layer.

- The standard deviation (σ_p) has been considered as the unique adjustable parameter; i.e. it is not chosen to accurately fit the "theoretical value" but to reproduce the SP electron density profiles. It is explained by the fact that, from SP solution, a weak penetration of the wave-functions in the oxide layer leads to a strong carrier repulsion. In contrast, in Monte-Carlo simulation corrected by an effective potential, a weak penetration of the distribution function assimilated to the particle wave-packet in the oxide layer originates a weak repulsive electric field close to the oxide/silicon interfaces, which therefore results in a weak carrier repulsion. That is why the standard deviation of the Pearson IV is not taken identical to the theoretical one but is generally taken slightly higher (cf. Fig. 4). More precisely, σ_p is chosen so that the Pearson penetration into the oxide layer induces a repulsive electric field which correctly reproduces electron density profile from SP simulation including several subbands.
- The skewness (γ) of the Pearson IV distribution has been chosen by fitting the theoretical one (cf. Fig. 4). The sign of the electric field determines the sign of the skewness (cf. Fig. 5e).
- The kurtosis (β) is arbitrarily calculated as a function of the skewness γ so as to be minimal and as close as possible to the Gaussian value (Selberherr, 1984; Sze, 1988).

Finally, this calibration procedure has allowed us to determine equations defining R_p, σ_p and γ as a function of E_x and T_{Si} as well as β as a function of γ (see 11. Appendix). This way, for each carrier position in the confinement direction, the associated Pearson IV distribution is fully defined (cf. Fig. 5b). It can be noted that the Pearson IV representing the wave-packet of a particle located at SiO_2/Si interfaces (x=0=x1 and x=T_{Si}=x5) is centred on $R_p \neq x$ and presents a noticeable asymmetry $\gamma \neq 0$. On the other hand, for a particle located at x=T_{Si}/2=x3, the Pearson IV looks like a Gaussian function (γ=0) and is centred on R_p=x=T_{Si}/2. With our new approach, all along the silicon film thickness and particularly close to the SiO_2/Si interfaces, the particle wave-packet representation is clearly more realistic than a Gaussian distribution. Moreover, since we have calibrated our PEP correction so as to reproduce electron density profiles resulting from SP calculation including 10 energy levels, one can say that our PEP correction integrates the description of valleys and of their associated subbands. However, this technique cannot include the confinement-induced redistribution of electrons among the different valleys as can be done in the Schrödinger-based correction method (Fan et al., 2004).

4.3 PEP calculation flowchart

The generic flowchart of the PEP calculation is presented in Fig. 6. As for the GEP correction, (i) the PEP correction has been implemented in the framework of a Monte-Carlo code (MONACO) (Saint-Martin et al., 2004), (ii) the parameter E_B = 3.1 eV is defined at the SiO_2/Si interfaces and satisfies $V_{oxide} = V_P - E_B$. E_x and T_{Si} being known, a set of four parameters (R_p, σ_p, γ, β) defining a Pearson IV distribution is calculated at each grid node of the structure as described in the previous section. Let us recall that the solution of Schrödinger's equation is not required for the PEP calculation. The Pearson IV determination

only needs the knowledge of calibrated parameters. The Pearson Effective Potential is then calculated at each position "x" as the integral (see eq. 2) of the product of the Poisson Potential with the associated Pearson IV distribution. Due to the different shapes of the Pearson IV distributions to be considered all along the silicon film thickness, the PEP correction can no longer be performed by a Fourier transform method as in the case of the GEP correction. It is now calculated using a Gaussian quadrature numerical integration method (Dhatt et al., 2005).

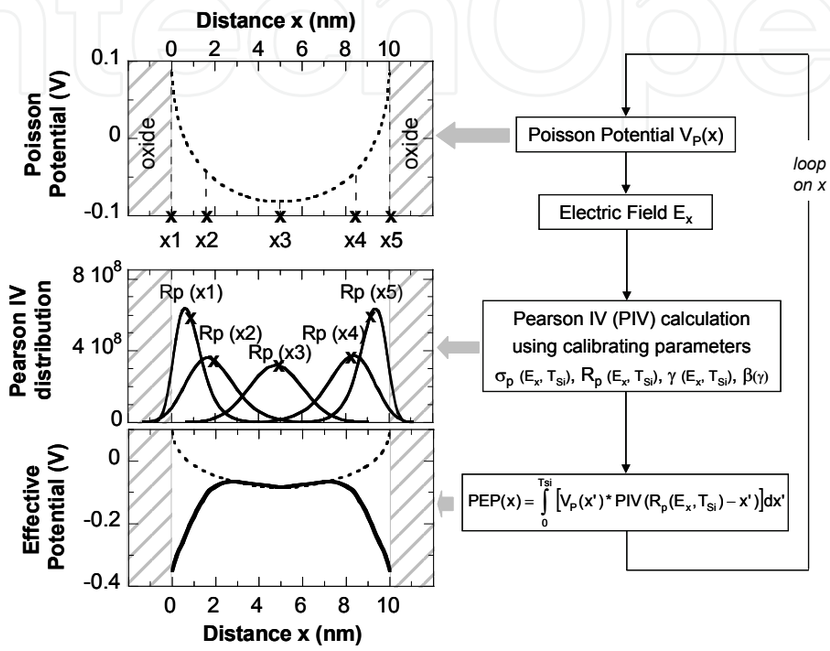

Fig. 6. Flowchart of the Pearson Effective Potential calculation illustrated by results on a double-gate device with T_{Si} =10 nm.

5. Pearson Effective Potential electrostatics validation

To validate the original PEP formulation, self-consistent simulations have been performed for several device architectures (double-gate, Silicon On Insulator (SOI) and bulk). Results of Monte-Carlo simulation corrected by the PEP model are compared with that obtained from SP calculation and GEP-corrected Monte Carlo simulation (with the value σ_x = 0.5 nm, as in (Akis et al., 2001 ; Palestri et al., 2005)). Because of confinement effects close to both SiO_2/Si interfaces, the double-gate nMOS architecture is one of the most critical devices to be tested to assess and demonstrate the ability of our PEP correction to reproduce the SP simulation results. The electron density profiles extracted from double-gate nMOS capacitors with 10 nm silicon film thickness and for a large range of effective fields (10^5 V.cm^{-1} ≤ E_{eff} ≤ 10^6 V.cm^{-1}) are shown in Figure 7a. While the electron density profiles calculated with the GEP correction are clearly unrealistic close to the Si/SiO_2 interfaces due to an unsuitable description of the particle wave-packet, those obtained by the PEP correction agree very well with SP results. Fig. 7b compares the Poisson potential resulting from the PEP correction (open circles) with that resulting from SP simulation (solid line). An excellent agreement is obtained between both approaches. The Poisson potential resulting from semi-

classical Monte-Carlo simulation (dotted line) and the Pearson Effective Potential which is actually responsible for the carrier movement (open squares) are also plotted in Fig. 7b. As expected the "quantum" Poisson potential exhibits a higher curvature than the "classical" one. Same results have been shown for double-gate nMOS capacitors with an oxide thickness T_{ox} varying from 0.5 nm up to 2 nm and a silicon film thickness T_{Si} ranging from 20 nm down to 5 nm without any changes in the Pearson IV parameters (Jaud et al., 2007a).

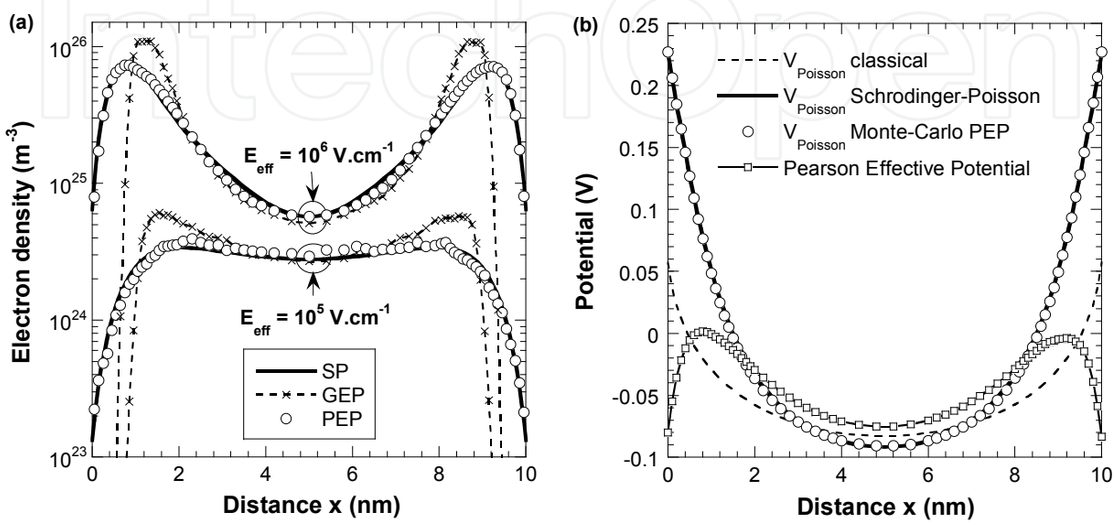

Fig. 7. (a) Electron density as a function of the distance in the confinement direction in a double-gate nMOS capacitor with $T_{Si} = 10$ nm, $T_{ox} = 1$ nm, $N_A = 10^{16}$ cm^{-3} and using SP (solid lines), GEP (cross dotted lines) and PEP (open circles) models. (b) Self-consistent Poisson Potential resulting from semi-classical (dotted line), SP (solid heavy line), Monte-Carlo with PEP correction (open circles) simulations and effective potential (PEP – open squares) as a function of the distance along the confinement direction extracted from the same capacitor.

Results obtained for a 5 nm silicon oxide thickness SOI capacitor and bulk nMOS capacitor with a channel doping $N_A = 10^{18}$ cm^{-3} and an oxide thickness $T_{ox} = 1$ nm are presented in Fig. 8. The simulations have been performed using the same calibrated parameters as for the double-gate structure. The electron density resulting from the PEP correction still properly reproduces SP results. Finally, the ability of the GEP and PEP quantum corrections to conserve the total inversion charge N_{inv} for double-gate, SOI and bulk devices is gathered in Table 1. The results of SP simulations are taken as reference. At high effective field, the total inversion charge N_{inv} is accurately reproduced with both approaches. In contrast, at low effective field, the PEP correction generates an error of more than 10% lower than that induced by the GEP. Thus, besides reproducing accurately the SP electron density profiles, the PEP correction also leads to inversion charge errors at the worst equal to the GEP ones or even considerably reduced.

All these results highlight that the PEP correction is well-suited to predict electrostatic quantum confinement effects in ultimate bulk, SOI or double-gate nMOS devices with various T_{Si}, T_{ox}, N_A and gate bias without any additional calibration. This "universality" mainly results from a judicious calibration of Pearson IV parameters as a function of the local electric field in the confinement direction and of the silicon film thickness.

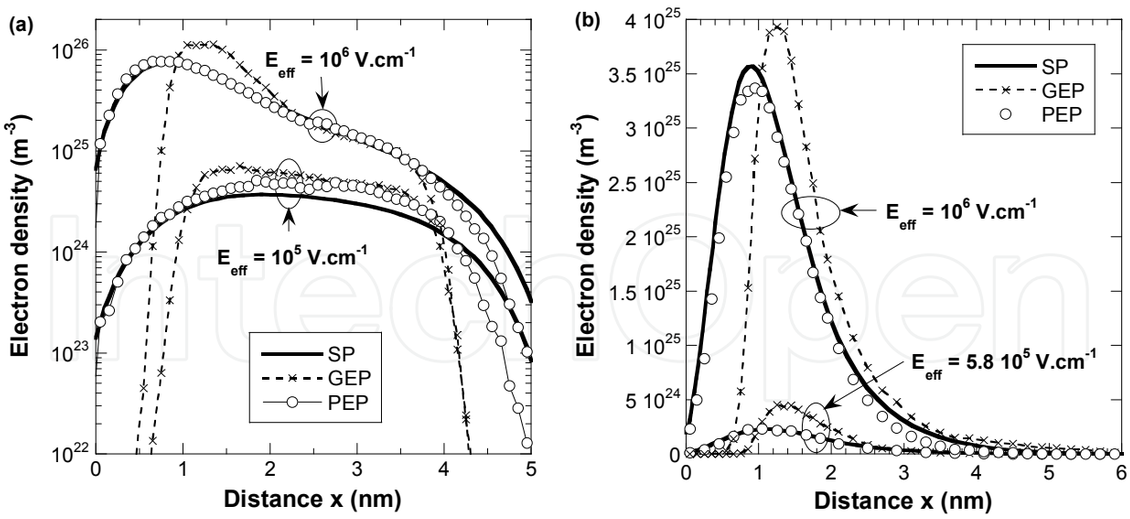

Fig. 8. Electron density as a function of the distance in the confinement direction in (a) a SOI nMOS capacitor with $T_{Si} = 5$ nm, $T_{ox} = 1$ nm, $N_A = 10^{16}$ cm^{-3} (b) a bulk nMOS capacitor with $T_{ox} = 1$ nm, $N_A = 10^{18}$ cm^{-3} and using SP (solid lines), GEP (cross dotted lines) and PEP (open circles) models.

nMOS capacitor			Monte-Carlo GEP		Monte-Carlo PEP	
Device	T_{Si} (nm)	T_{ox} (nm)	Low E_{eff}	High E_{eff}	Low E_{eff}	High E_{eff}
DG	20	1	11.0	2.8	0.7	0.4
DG	15	1	11.6	5.7	0.2	2.7
DG	10	1	17.1	1.9	4.8	1.6
DG	8	1	21.0	5.1	6.8	0.8
DG	5	1	32.2	1.8	21.6	3.9
DG	10	2	13.3	1.1	2.3	1.1
DG	10	0.5	23.2	4.1	5.6	2.7
SOI	10	1	24	3	1.6	0.7
SOI	5	1	35	2.3	23	2.3
Bulk		1	23.5	13.1	7.87	9.7

Table 1. Inversion charge error (in percentage) for various nMOS capacitors. Low E_{eff} corresponds to 10^5 V.cm^{-1} for double-gate (DG) and SOI devices and to 5.8×10^5 V.cm^{-1} for bulk devices. High E_{eff} corresponds to 10^6 V.cm^{-1}.

6. Quantum correction for Monte-Carlo device simulation

6.1 Simulated device

The simulated device is a double-gate nMOSFET with a channel length $L_C = 10$ nm, a SiO_2 oxide thickness $T_{ox} = 1.1$ nm and a silicon thickness $T_{Si} = 5$ nm. Not only the channel but also the source and drain regions are covered with SiO_2 oxide material. The source and drain regions are uniformly doped to 10^{20} cm^{-3} and the P-type residual doping level in the channel

is 10^{15} cm^{-3}. The metallic gate work function (ϕ_M = 4.56 eV) corresponds to midgap material. The scattering mechanisms included in the model are the acoustic intravalley phonon scattering, three *f* and three *g* intervalley phonons scattering, and the electron-impurity scattering. In all simulations, the phonon scattering is computed via bulk-phonons using the same coupling constants that for 2D and 3D electron gas (Saint-Martin et al., 2006). To make easier the comparison between semi-classical, quantum corrected and multi-subband Monte-Carlo simulations with strictly similar scattering models, surface roughness scattering is not included here. Finally, degeneracy effects are not included in this work.

6.2 Treatment of quantization effects in source and drain

The simulation of the device presented above requires to considering quantum correction not only in the channel area but also in the source and drain areas where quantum confinement between oxide barriers also occurs. In these source and drain areas, and more generally in the case of a quasi-flat band potential profile in the confinement direction, the PEP correction consists in preserving the Gaussian distribution characteristic of the flat-band regime, but with an average position evolving at a small distance around the middle of the silicon film. This distance and the standard deviation of the Gaussian distribution are calibrated only as a function of the silicon film thickness.

To study the transition between the flat-band and the usual PEP corrections, the electron density profiles in the source-to-drain direction (referred to as *y*-axis) of an nMOS capacitor resulting from SP and PEP simulations are shown in Fig. 9. No discontinuity is observed at the source/channel junction. Moreover, a very good agreement is conserved between SP and PEP electron density profiles.

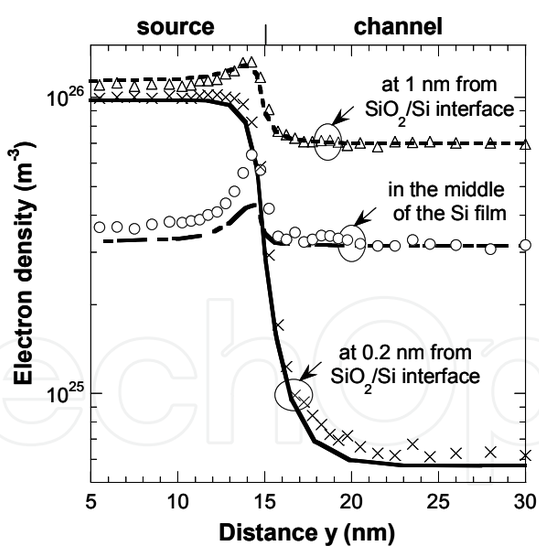

Fig. 9. Electron density profiles extracted in different slices along the transport direction close to the source/channel junction of a double-gate nMOS capacitor in inversion regime for SP (lines) and PEP model (symbols). T_{Si} = 10 nm.

6.3 Boundary conditions at source and drain contacts

In a usual semi-classical Monte-Carlo approach, the charge neutrality conditions on plane ohmic contact are applied, that is not well-suited with quantum confinement effects in

source and drain areas. Thus, the following procedure has been adopted. The potential profile along x axis in the middle of the drain area (where boundary conditions do not affect the potential) is applied to the drain contact for Poisson's equation solution. The corresponding boundary condition, i.e. the potential profile applied at the source contact, is the same as at the drain contact but shifted by the drain to source voltage.
To conclude this section, thanks to the 1D PEP correction extended to the flat-band regime with the well-suited boundary conditions, the carrier quantum confinement is correctly described in the full nMOSFET structure.

7. PEP corrected vs. multi-subband Monte-Carlo

In this section the results obtained from semi-classical, GEP corrected, PEP corrected and multi-subband Monte-Carlo are compared. As for GEP and PEP, Multi-Subband Monte-Carlo (MSMC) approach (Saint-Martin et al., 2006) has been implemented in the framework of the MONACO code. Contrary to the GEP and PEP corrections, the MSMC solves the Schrödinger equation in the confinement direction and considers that all carriers are confined in a 2D gas. As a consequence, multi-subband (respectively GEP and PEP corrected) Monte-Carlo assumes 2D (respectively 3D) scattering rates and carrier movement. The MSMC approach is based on the mode-space approximation of decoupled 2D subbands only coupled by inter-subband scattering. This approximation is proved correct for ultra-thin double-gate structures ($T_{Si} < 10$ nm) (Sverdlov et al., 2005). It may become questionable for structures where the subband coupling should be considered in the Schrödinger equation as in (Bulk or SOI) single-gate devices, and it cannot be easily applied in thicker devices since a dramatically large number of subbands and/or a tricky coupling with a 3D continuum of states should be required. In the present work, the MSMC approach has been performed for the 5 nm silicon film thickness double-gate nMOSFET previously described. In the following, electrical characteristics and then microscopic quantities are carefully compared at low and high drain voltages.
It should be noted that the GEP corrected, PEP corrected and multi-subband Monte-Carlo methods induce a computation-time multiplied by 2, 10 and 30 compared to that of semi-classical Monte-Carlo, respectively.

7.1 Current-voltage characteristics

The electrical output characteristics $I_{DS}(V_{GS})$ calculated at $V_{DS} = 0.05$ V and $I_{DS}(V_{DS})$ calculated at $V_{GS} = 1.2$ V resulting from semi-classical, GEP corrected, PEP corrected and multi-subband Monte-Carlo simulations are shown in Fig. 10. This figure demonstrates the limitations of the GEP correction to properly include quantization effects: it is not only unable to accurately reproduce electrostatic quantum confinement effects but it also over corrects the current, which yields an underestimation of the drain current by more than 10% with respect to the MSMC results used as reference. Accordingly, the GEP correction is no longer considered in this work. In contrast, the PEP correction provides excellent results.
The total electron charge extracted at $V_{DS} = 0.05$ V and $V_{DS} = 0.7$ V as a function of the gate voltage and resulting from semi-classical, PEP corrected and multi-subband Monte-Carlo simulations is plotted in Fig. 11a. At the same drain voltages and at $V_{GS} = 1.2$ V, Fig. 11b represents the electron charge all along the device in the transport direction. It is remarkable that for all quantities plotted in Figs. 10-11 the PEP results fit in very well with multi-

subband ones. In Fig. 10, we observe a reduction of drive current when quantum confinement effects are included (by 6.2% with PEP at $V_{GS} = 1.2$ V and $V_{DS} = 0.7$ V). It is mainly explained by a smaller effective gate capacitance due to carrier repulsion at the SiO_2/Si interfaces (cf. Fig. 11) inducing a reduction of inversion charge at given bias.

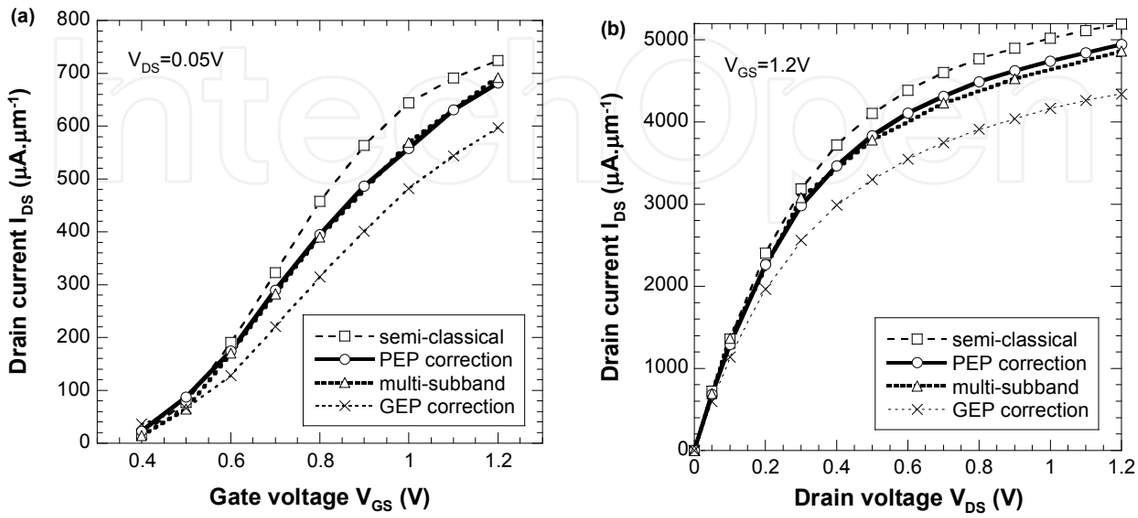

Fig. 10. Output I_{DS}-V_{GS} characteristics at $V_{DS} = 0.05$ V (a) and output I_{DS}-V_{DS} characteristics at $V_{GS} = 1.2$ V (b) resulting from semi-classical (squares), PEP corrected (circles), multi-subband (triangles) and GEP corrected (crosses) Monte-Carlo simulations.

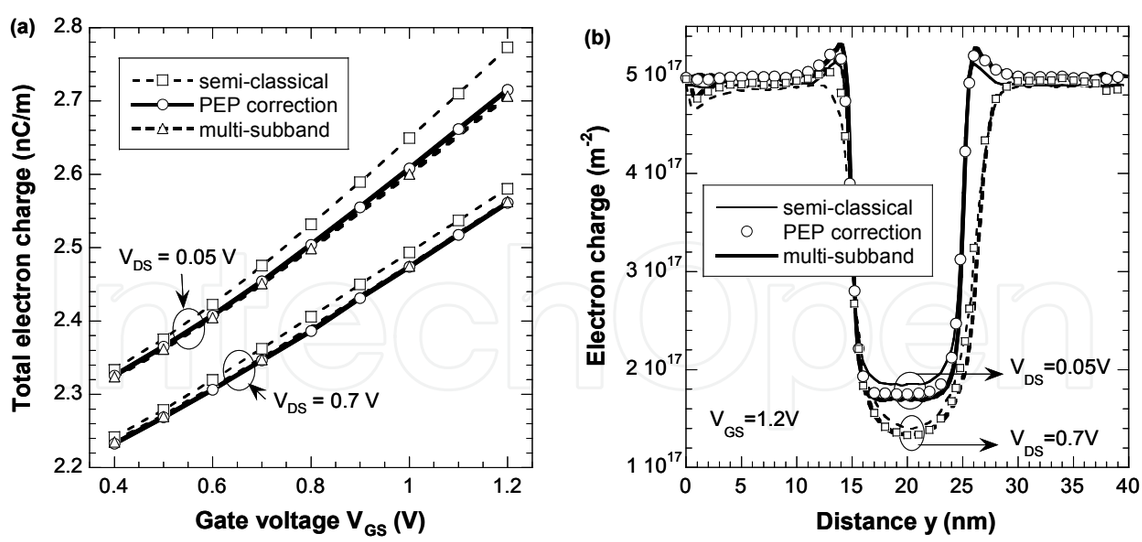

Fig. 11. (a) Total electron charge as a function of the gate voltage V_{GS} for $V_{DS} = 0.05$ V and $V_{DS} = 0.7$ V resulting from semi-classical (squares), PEP corrected (circles) and multi-subband (triangles) Monte-Carlo. (b) Electron charge (electron density integrated over the silicon film thickness) along the transport direction for $V_{DS} = 0.05$ V and $V_{DS} = 0.7$ V resulting from semi-classical (thin lines), PEP corrected (symbols) and multi-subband (thick lines) Monte-Carlo. $V_{GS} = 1.2$ V.

7.2 Microscopic quantities

Cartographies of electron density obtained by PEP corrected Monte-Carlo simulations at $V_{DS} = 0.05$ V and $V_{GS} = 1.2$ V and at $V_{DS} = 0.7$ V and $V_{GS} = 0.8$ V are shown in Figs. 12a and 13a, respectively.

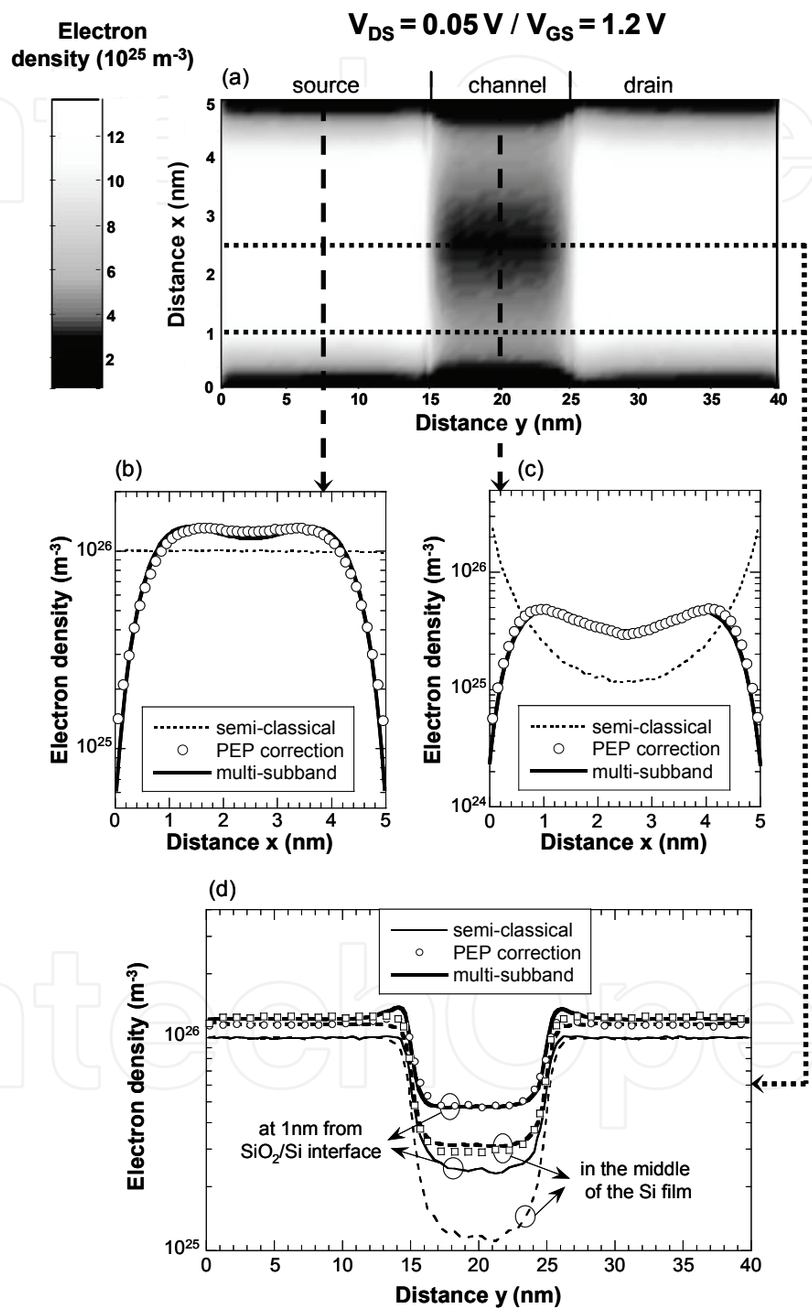

Fig. 12. Cartography of the electron density resulting from the PEP correction at $V_{GS} = 1.2$ V and $V_{DS} = 0.05$ V (a). Electron density profiles extracted in different slices of the device along either gate-to-gate (b-c) or source-drain (d) directions for semi-classical (thin lines), PEP corrected (symbols) and multi-subband Monte-Carlo (thick lines) simulations.

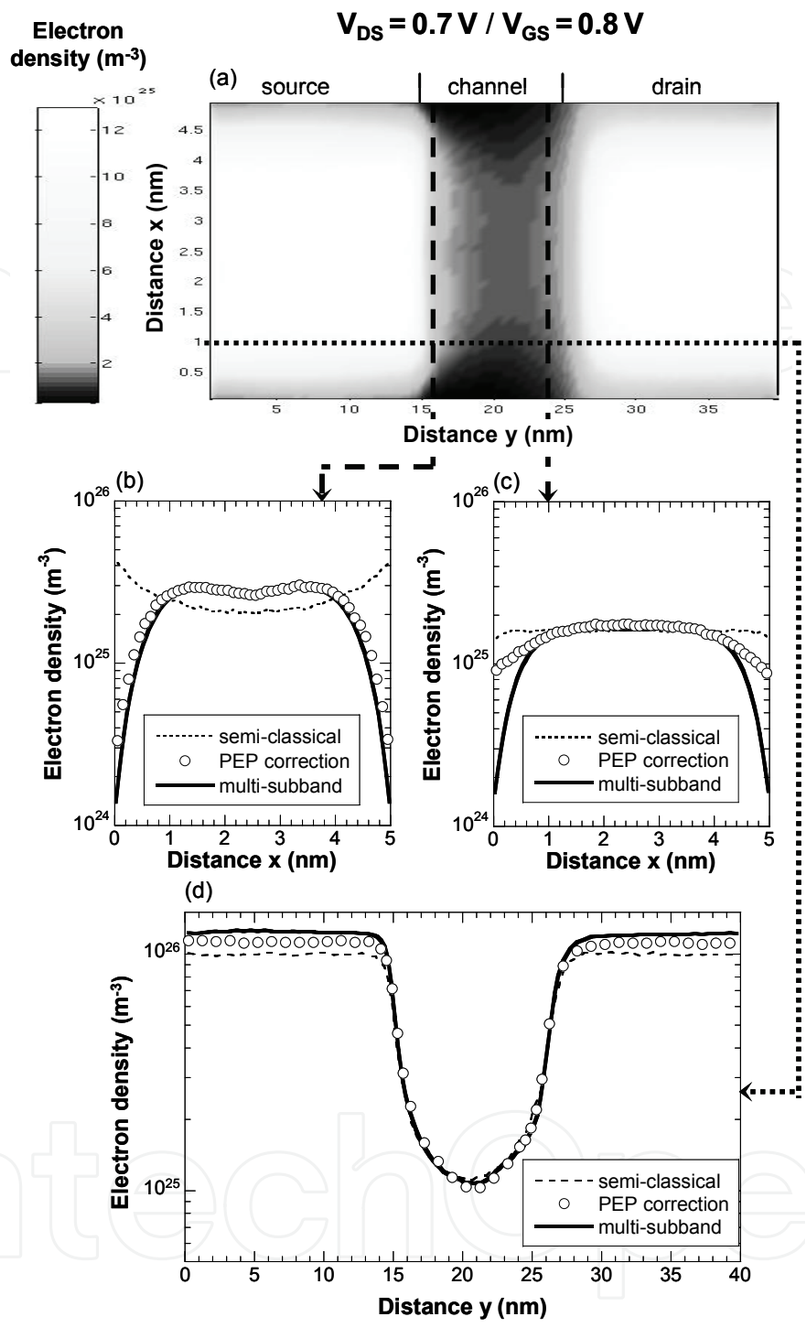

Fig. 13. As in Fig. 12 at V_{GS} = 0.8 V and V_{DS} = 0.7 V for semi-classical (thin dotted lines), PEP corrected (open circles) and multi-subband Monte-Carlo (thick solid lines) simulations.

At these same applied voltages, we also compare electron density and potential profiles resulting from semi-classical, PEP correction and multi-subband Monte-Carlo simulation along the confinement and the transport directions (cf. Figs. 12b-12d ; 13b-13d). First of all, comparisons with semi-classical results highlight the impact of quantum confinement effects. At low drain voltage, two maxima of density at about 1 nm from the Si/SiO_2 interfaces are observed (cf. Figs. 12a-12c). Figs. 13a-13c show a gradual reduction of the

confinement effects along the channel under high drain voltage. It is mainly explained by the curvature of the conduction band that is less sensitive to the drain voltage at the source-end of the channel than at the drain-end. In most cases, excellent agreement is found between PEP and multi-subband electron density profiles all along the device. However, at the drain end of the channel and under high drain voltage (cf. Fig. 13c), the electron repulsion at the Si/SiO_2 interfaces induced by the PEP correction is less pronounced than that induced by MSMC. Such behavior may be related to carrier heating in this channel region, which is observable in Fig. 14a where the electron kinetic energy averaged in the confinement direction is plotted as a function of the source-to-drain distance. Indeed, in MSMC simulation, high electric field induces electron heating which redistributes carriers by phonon scattering within higher subbands with envelope functions different from that of the low-field case. In contrast, using the PEP correction even if the same "quantum" potential barrier is seen by both thermal and hot electrons, hot electrons are allowed to get closer to the oxide interfaces than thermal ones. To still improve the PEP model, an additional correction is probably needed to better describe the repulsive effect for high energy carriers. Besides, kinetic energy resulting from semi-classical and PEP corrected Monte-Carlo are quite similar and higher than that resulting from MSMC. This is consistent with the fact that energy of carriers at thermal equilibrium in a 2D electron gas is k_BT_e instead of $3/2\ k_BT_e$ in a 3D electron gas (with k_B the Boltzmann constant and T_e the electron temperature). However, it should be nicely observed that this error does not really affect the inversion charge. This conservation combined with the additional excellent agreement obtained on the average velocity profile plotted in Fig. 14b consistently explains the good concordance on drain currents calculated with both approaches (cf. Fig. 10).

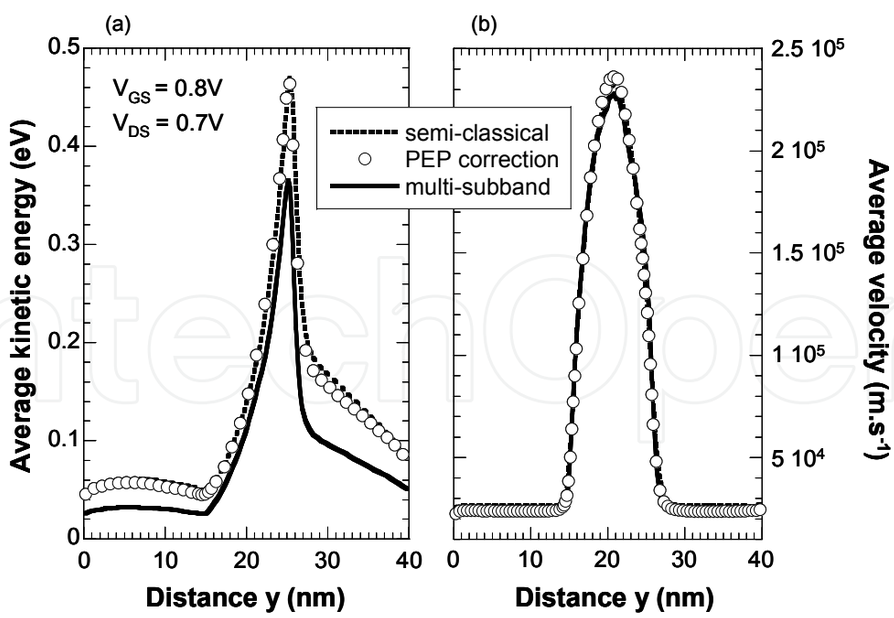

Fig. 14. Kinetic energy (a) and velocity (b) averaged over the confinement direction (semi-classical and PEP correction) or over the different subbands (multi-subband) according to carrier density at V_{GS} = 0.8 V and V_{DS} = 0.7 V resulting from semi-classical (dotted lines), PEP corrected (open circles) and multi-subband (solid lines) Monte-Carlo simulations.

Moreover, velocity obtained from PEP and multi-subband Monte-Carlo models are similar to the semi-classical one. Contrary to the electrostatics in the confinement direction, the transport properties in the source-to-drain direction are not significantly affected by quantum confinement effects in the case of very thin silicon film.
Finally, the very good overall agreement on both electrical characteristics and microscopic quantities between PEP corrected and multi-subband Monte-Carlo approaches for a very aggressive double-gate MOSFET largely validates the PEP correction. Similar results have been obtained on a double-gate nMOSFET with a channel length $L_C = 20$ nm and a silicon thickness $T_{Si} = 8$ nm (Jaud et al, 2007b). By means of comparisons with semi-classical Monte-Carlo results, the PEP correction can now be used to further study the impact of quantum confinement effect on electron transport and device performances depending on design parameters.

8. Impact of the quantum confinement effects

In this section, the simulated devices are double-gate nMOSFETs with a silicon film thickness $T_{Si} = 5$ nm and a channel length L_C varying from 10 up to 40 nm and double-gate nMOSFETs with $L_C = 20$ nm and T_{Si} varying from 5 up to 10 nm. The drive current I_{DS} resulting from semi-classical and PEP corrected Monte-Carlo simulations and extracted at V_{GS}-V_{th} = V_{DS} = V_{DD} = 0.7 V is plotted in Fig. 15 as a function of L_C and T_{Si} where V_{th} is the threshold voltage obtained at low V_{DS} for each device.

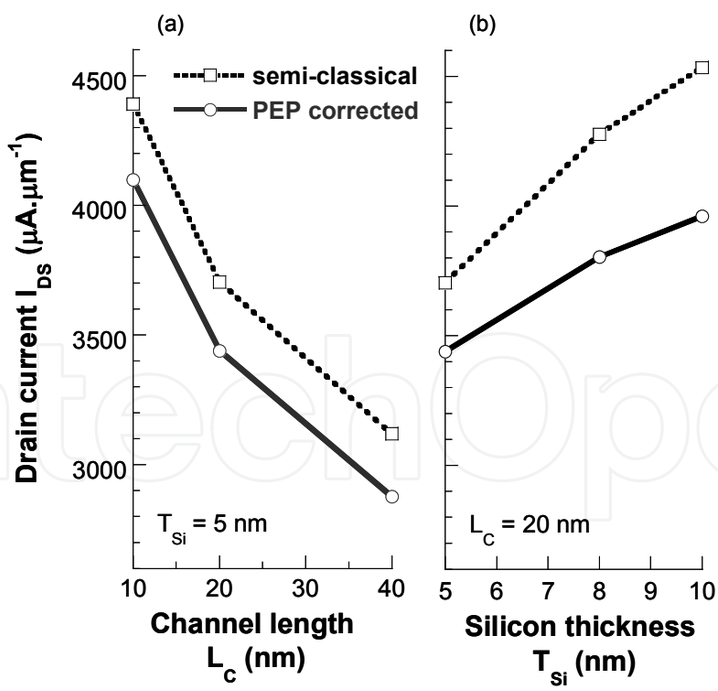

Fig. 15. Drain current I_{DS} resulting from semi-classical (dotted lines) and PEP corrected (full lines) Monte-Carlo simulations and obtained at V_{GS}-V_{th} = V_{DS} = V_{DD} = 0.7 V on double-gate nMOSFET as a function of the channel length L_C (T_{Si} = 5 nm) (a) and the silicon film thickness T_{Si} (L_C = 20 nm) (b).

At these same bias, we plot the inversion charge N_{inv} and the velocity v_{inj} extracted at the maximum of the potential energy (averaged in the confinement direction according to carrier density) obtained on the previous devices with $T_{Si} = 5$ nm (cf. Fig. 16) and $L_C = 20$ nm (cf. Fig. 17) for semi-classical and PEP corrected Monte-Carlo as a function of the drive current I_{DS}. For all simulated devices, quantum confinement effects induce a decrease of drive current lower than 13% compared to semi-classical results (cf. Fig. 15), which is mainly attributed to the decrease of the inversion charge. When the channel length is decreased we observe a raise of the drive current I_{DS} (cf. Fig. 15a) that presents a linear correlation with the increase of the average velocity at the top of the barrier while the inversion charge N_{inv} is nearly independent on L_C (cf. Fig. 16). This increase of injection velocity is directly related to the reduced backscattering in the channel.

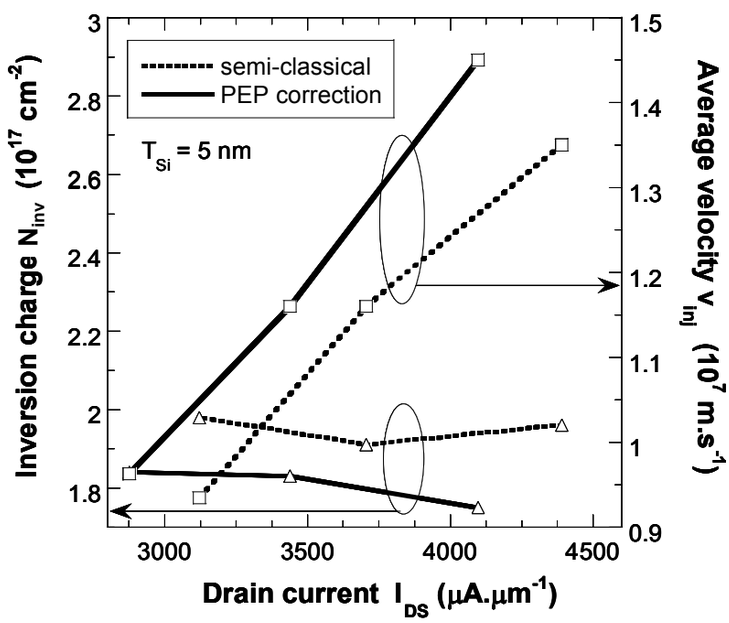

Fig. 16. Inversion charge (triangles) and average velocity (squares) as a function of the drain current I_{DS} resulting from semi-classical (dotted lines) and PEP corrected (full lines) Monte-Carlo simulations and obtained at V_{GS}-V_{th} = V_{DS} = V_{DD} = 0.7 V on double-gate nMOSFET with different channel lengths L_C at given $T_{Si} = 5$ nm. The inversion charge and the average velocity have been extracted at the maximum of the potential energy (averaged over the confinement direction according to carrier density).

When the silicon film thickness is increased we observe an increase of the drive current I_{DS} (cf. Fig. 15b), that presents a linear correlation with the increase of the inversion charge at the top of the barrier (cf. Fig. 17). This behavior of the inversion charge is a direct consequence of the thinning-induced enhancement of source-access resistance which weakens the gate control of the channel. Surprisingly enough, when the silicon film thickness is reduced (cf. Fig. 15b), the impact of quantum confinement effects becomes less important and the drop of drive current is about 7% for $T_{Si} = 5$ nm. The increase of the inversion charge distribution in the middle of the film partly compensates the carrier

depletion near the Si/SiO_2 interfaces, which explains this trend. For 5 nm silicon film thickness, the reduction of drive current due to quantum confinement effects is not very sensitive to the channel length L_C (cf. Fig. 15a); this drive current reduction only slightly increases when L_C increases.

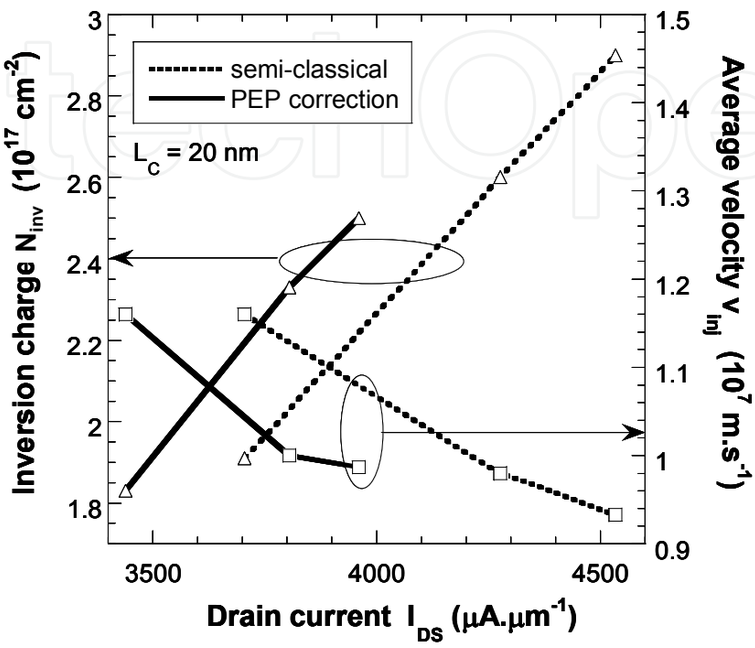

Fig. 17. As in Fig. 16 but obtained on double-gate nMOSFET with different silicon film thicknesses T_{Si} at given L_C = 20 nm.

9. Conclusion

The new Pearson Effective Potential scheme has been developed to account for quantum confinement effects in nano-scaled devices and has been implemented into a semi-classical Monte-Carlo simulator. It mainly consists of an improvement of the particle wave-packet description: the Gaussian distribution used in the usual GEP correction is replaced by a Pearson IV distribution that can much better fit the square modulus of the ground subband Schrödinger wave function. Thanks to a judicious calibration of Pearson IV parameters dependent on the silicon film thickness and local electric field in the confinement direction, the PEP correction accurately predicts electrostatic quantum confinement effects in ultimate bulk, SOI or double-gate nMOS and properly describes the impact of quantum confinement on electron transport in terms of both electrical characteristics and microscopic quantities. Indeed, excellent agreement between quantum corrected and multi-subband Monte-Carlo simulations are shown on a nano-scaled double-gate nMOSFET. Comparisons between semi-classical and PEP corrected Monte-Carlo simulations on nano-scaled double-gate nMOSFETs show that the reduction of the inversion charge induced by quantum confinement effects are mainly responsible for a decrease of about 10% on the drive current.

Finally, the PEP correction can be easily extended to several confinement directions and is well suited for the simulation of various nMOSFET architectures such as double-gate, silicon on insulator or bulk.

10. Acknowledgements

This work was supported by the Agence Nationale pour la Recherche through project MODERN (ANR-05-NANO-002).

11. Appendix: Pearson IV definition and PEP calibration

The Pearson IV distribution is defined as (Selberherr, 1984 ; Sze, 1988):

$$f(x) = K\left[b_0 + b_1(x - R_P) + b_2(x - R_P)^2\right]^{\frac{1}{2b_2}}$$
$$\exp\left[-\frac{\frac{b_1}{b_2} + 2b_1}{\sqrt{4b_0b_2 - b_1^2}}\, a\tan\left(\frac{2b_2(x - R_P) + b_1}{\sqrt{4b_0b_2 - b_1^2}}\right)\right] \tag{3}$$

with b_0, b_1 and b_2 given by:

$$b_0 = -\frac{\sigma_P^2\left(4\beta - 3\gamma^2\right)}{10\beta - 12\gamma^2 - 18}$$

$$b_1 = -\frac{\gamma\ \sigma_P(\beta + 3)}{10\beta - 12\gamma^2 - 18} \tag{4}$$

$$b_2 = -\frac{2\beta - 3\gamma^2 - 6}{10\beta - 12\gamma^2 - 18}$$

and K is a constant to ensure that the Pearson IV is normalized.
The skewness γ and the kurtosis β obey the following conditions:

$$0 < \gamma^2 < 32 \tag{5}$$

$$\beta > \frac{39\gamma^2 + 48 + 6\left(\gamma^2 + 4\right)^{\frac{3}{2}}}{32 - \gamma^2} \tag{6}$$

We recall that the average position R_P, the standard deviation σ_P, the skewness γ and the kurtosis β are defined as a function of the first four moments of the distribution function as following:

$$R_P = \mu_1 \qquad \sigma_P = \sqrt{\mu_2} \qquad \gamma = \frac{\mu_3}{\mu_2^{3/2}} \qquad \beta = \frac{\mu_4}{\mu_2^{2}} \tag{7}$$

In our PEP correction, the wave-packet of a particle located in "x" in the confinement direction and under an electric field E_x is represented by a Pearson IV distribution whose moments have been calibrated as a function of E_x and T_{Si}. We present here the expressions of each of the four calibrated Pearson IV moments. Table 2 gathers all the notations specifying their unit and significance. The parameters' values necessary for Pearson moments calculation are listed in Table 3.

Name	Unit	Definition
α_1	m^{-1}	Constant parameter for σ_P calculation $\alpha_1=10^9$ m^{-1}
α_2	m^{-1}	Constant parameter for σ_P calculation $\alpha_2=17.10^{11}$ m^{-1}
β		Kurtosis (cf. eq. 12)
$\lvert E_X \rvert$	$V.m^{-1}$	Local electric field in the confinement direction
$\lvert E_X \rvert_{max}$	$V.m^{-1}$	Constant parameter $\lvert E_X \rvert_{max}= 3.5\ 10^8$ $V.m^{-1}$
γ	ad.	Skewness (cf. eq. 11)
γ_{max}	ad.	Parameter for γ calculation (cf. Table 3)
R_P	m	Average position (cf. eq. 9)
R_{Pa}	ad.	Parameter for R_P calculation (cf. Table 3)
R_{Pdiv}	m	Parameter for R_P calculation (cf. Table 3)
R_{Pmax}	ad.	Parameter for R_P calculation (cf. Table 3)
R_{P0}	m	Average position of a carrier under a zero electric field E_x
R_{P1}	m	Average position of a carrier located at the 1st interface (cf. eq. 8)
R_{P2}	m	Average position of a carrier located at the 2nd interface (cf. eq. 8)
σ_P	m	Standard deviation (cf. eq. 10)
T_{Si}	m	Silicon film thickness
T_{Sis}	ad.	Parameter for σ_P calculation (cf. Table 3)
x1	m	Location of the 1st interface
x2	m	Location of the 2nd interface

Table 2. Unit and significance of all the notations used for the calculation of the Pearson IV calibrated parameters (ad. is for adimensional).

Average position

The average position is calculated in two different steps. Firstly, the average position of a particle located at the first interface (R_{P1}) and at the second interface (R_{P2}) are calculated as a function of E_x and T_{Si} so as to fit the theoretical values:

$$R_P = \frac{T_{Si}}{2} - \frac{1}{\log(10^{R_{Pa}})}\left(\frac{T_{Si}}{2} - R_{P\max}\right) \times \log\left[\frac{10^{R_{Pa}} \times |E_x|}{|E_x|_{\max}} + 1\right] \tag{8}$$

Moreover, for a particle under a zero electric field, the average position of its wave-packet (R_{P0}) is equal to its location. Secondly, for each particle location, the average position of its wave-packet R_P is calculated from R_{P0}, R_{P1} and R_{P2} while ensuring that $R_P(x)$ is continuous and regular:

$$\begin{aligned} &\text{If} \quad x \le R_{P0} \\ &\text{then} \qquad R_P = R_{P0} + (R_{P0} - R_{P1} - x_1).\frac{\tanh\left(\frac{(x - R_{P0})}{R_{Pdiv}}\right)}{\left|\tanh\left(\frac{(x_1 - R_{P0})}{R_{Pdiv}}\right)\right|} \\ &\text{else} \qquad R_P = R_{P0} - (R_{P0} + R_{P2} - x_2).\frac{\tanh\left(\frac{(x - R_{P0})}{R_{Pdiv}}\right)}{\left|\tanh\left(\frac{(x_2 - R_{P0})}{R_{Pdiv}}\right)\right|} \end{aligned} \tag{9}$$

Standard deviation

For a particle under a local electric field in the confinement direction E_x, the standard deviation of the Pearson IV representing its wave-packet is calculated as follows:

$$\sigma_P = \frac{1}{\alpha_1} \times \left[\log(T_{Sis}) + \frac{T_{Sis} + 1.5}{50}\right] - \frac{1}{\alpha_2} \times (T_{Sis})^3 \times \log\left[\frac{(-8 \times T_{Sis} + 90) \times |E_x|}{|E_x|_{\max}} + 1\right] \tag{10}$$

Skewness

The skewness is calculated as a function of E_x and T_{Si} so as to fit the theoretical values:

$$\gamma = \gamma_{\max} \times \tanh\left[\frac{T_{Si}}{10^{-9}} \times \frac{|E_x|}{|E_x|_{\max}}\right] \tag{11}$$

Moreover, the sign of the skewness is then adjust to be in adequacy with the sign of the local electric field in the confinement direction E_x.

Kurtosis

In accordance with Pearson IV definition (Selberherr, 1984 ; Sze, 1988), the kurtosis is only calculated as a function of the skewness γ so as to be minimal and closest to the Gaussian value:

$$\beta = \frac{39\gamma^2 + 48 + 6\left(\gamma^2 + 4\right)^{\frac{3}{2}}}{32 - \gamma^2} + \varepsilon \tag{12}$$

with ε>0 to prevent from numerical difficulties.

Name	T_{Si} < 10 nm	$T_{Si} \geq$ 10 nm
γ_{max}	$0.03xT_{Si}/10^{-9} + 0.6$	0.9
R_{Pa}	5	Integer part $[0.7xT_{Si}/10^{-9} - 2]$
R_{Pdiv}	$6\ 10^{-9}$	$0.4xT_{Si} + 2\ 10^{-9}$
R_{Pmax}	$-0.034xT_{Si} + 1.17\ 10^{-9}$	$0.83\ 10^{-9}$
T_{Sis}	$T_{Si}/10^{-9}$	10

Table 3. Values of the parameters as a function of T_{Si} used for Pearson IV calibrated parameters calculation according to the units defined in Table 2.

12. References

Ahmed et al., 2005 : S.S. Ahmed, C. Ringhofer, D. Vasileska, Parameter-Free Effective Potential Method for Use in Particle-Based Device Simulations, *IEEE Transactions on Nanotechnology*, vol. 4, pp. 465-471, 2005.

Akis et al., 2001 : R. Akis, N. Milicic, D. K. Ferry, D. Vasileska, An effective potential method for including quantum effects into the simulation of ultra-short and ultra-narrow channel MOSFETs, *International conference on Modeling and Simulation of Microsystem (MSM 2001)*, vol. 1, pp. 550-553, 2001.

Bohm, 1952: D. Bohm, A suggested interpretation of the quantum theory in terms of "Hidden" variables. II, *Physical Review*, vol. 85, pp. 180-193, 1952.

Dhatt et al., 2005 : G. Dhatt, G. Touzot, E. Lefrançois, Méthode des élements finis, *Hermes Science Publications*, pp. 345-383, 2005.

Fan et al., 2004 : X.-F Fan, X. Wang, B. Winstead, L. F. Register, U. Ravaioli, S. Banerjee, MC simulations of Strained-Si MOSFET with Full-Band Structure and Quantum Correction, *IEEE Transaction on Electron Devices*, vol. 51, pp. 962-970, 2004.

Ferry et al., 2000 : D.K. Ferry, R. Akis, D. Vasileska, Quantum effects in MOSFETs: Use of an Effective Potential in 3D Monte Carlo Simulation of Ultra-Short Channel Devices, *IEDM Technical Digest*, pp. 287-290, 2000.

Feynman & Hibbs, 1965 : R.P. Feynman and A. R. Hibbs, Quantum mechanics and path integrals, *McGraw-Hill Publishing Company*, pp. 267-286, 1965.

Jaud et al., 2006 : M.-A. Jaud, S. Barraud, P. Dollfus, H. Jaouen, F. de Crecy and G. Le Carval, Validity of the effective potential approach for the simulation of quantum confinement effects: A Monte-Carlo study, *Journal of Comput. Electron.*, vol. 5, pp. 171-175, 2006.

Jaud et al., 2007a : M.-A. Jaud, S. Barraud, P. Dollfus, H. Jaouen and G. Le Carval, Pearson versus gaussian effective potentials for quantum-corrected Monte-Carlo simulation, *Journal of Comput. Electron.*, vol. 6, pp. 19-22, 2007.

Jaud et al., 2007b : M.-A. Jaud, S. Barraud, J. Saint-Martin, A. Bournel, P. Dollfus and H. Jaouen, Pearson Effective Potential vs. Multi-Subband Monte-Carlo Simulation for Electron Transport in DG nMOSFET, *in Proc. SISPAD 2007, Springer*, pp. 65-68, 2007.

Jaud et al., 2008 : M.-A. Jaud, S. Barraud, J. Saint-Martin, A. Bournel, P. Dollfus and H. Jaouen, A Pearson Effective Potential for Monte-Carlo simulation of quantum confinement effects in nMOSFETs, *IEEE Transactions on Electron Devices*, vol. 55, pp. 3450-3458, 2008.

Li et al., 2002 : Y. Li, T.-W. Tang and X. Wang, Modeling of quantum effects for ultrathin oxide MOS structures with an effective potential, *IEEE Transactions on Nanotechnology*, vol. 1, pp. 238-242, 2002.

Lucci et al., 2005 : L. Lucci, P. Palestri, D. Esseni, L. Selmi, Multi-subband Monte Carlo modeling of nano-MOSFETs with strong vertical quantization and electron gas degeneration, *IEDM Tech. Dig.*, pp. 617-620, 2005.

Madelung, 1926 : E. Madelung, Quantatheorie in hydrodynamischer form, *Z. Phys.*, vol. 40, pp. 322-326, 1926

Nedjalkov et al., 2004 : M. Nedjalkov, H. Kosina, S. Selberherr, C. Ringhofer, D. K. Ferry, Unified particle approach to Wigner-Boltzmann transport in small semiconductor devices, *Physical Review B*, vol. 70, p. 115319, 2004.

Palestri et al., 2005 : P. Palestri, S. Eminente, D. Esseni, C. Fiegna, E. Sangiorgi, L. Selmi, An improved semi-classical Monte-Carlo approach for nano-scale MOSFET simulation, *Solid-State Electronics*, vol. 49, pp. 727-732, 2005.

Querlioz et al., 2006 : D. Querlioz, P. Dollfus, V.-N. Do, A. Bournel and V. Lien Nguyen, An improved Wigner Monte-Carlo technique for the self-consistent simulation of RTDs, *Journal of Computational Electronics*, vol. 5 pp. 443-446, 2006.

Querlioz et al., 2007 : D. Querlioz, J. Saint-Martin, K. Huet, A. Bournel, V. Aubry-Fortuna, C. Chassat, S. Galdin-Retailleau and P. Dollfus, On the ability of the particle Monte Carlo technique to include quantum effects in nano-MOSFET simulation, *IEEE Transaction on Electron Devices*, vol. 54, pp. 2232-2242, 2007.

Riolino et al., 2006 : I. Riolino, M. Braccioli, L. Lucci, D. Esseni, C. Fiegna, P. Palestri and L. Selmi, Monte-Carlo simulation of decananometric double-gate SOI devices: Multi-subband vs. 3D electron gas with quantum corrections, *ESSDERC Tech. Digest.*, pp. 162-165, 2006.

Saint Martin et al., 2004 : J. Saint-Martin, A. Bournel and P. Dollfus, On the ballistic transport in nanometer scaled DGMOSFET, *IEEE Transactions on Electron Devices*, vol. 51, pp. 1148-1155, 2004.

Saint Martin et al., 2006 : J. Saint-Martin, A. Bournel, F. Monsef, C. Chassat and P. Dollfus, Multi sub-band Monte Carlo simulation of an ultra-thin double-gate MOSFET with 2D electron gas, *Semiconductor Science and Technology*, vol. 21, L29-L31, 2006.

Selberherr, 1984 : S. Selberherr, Analysis and simulation of semiconductor devices, *Springer-Verlag Wien New-York*, p. 46 and following, 1984.

Shifren et al., 2003 : L. Shifren, C. Ringhofer and D. K. Ferry, A Wigner Function-Based Quantum Ensemble Monte-Carlo study of a Resonant Tunneling Diode, *IEEE Transactions on Electron Devices*, vol. 50, pp. 769-773, 2003.

Sverdlov et al., 2005 : V. Sverdlov, A. Gehring, H. Kosina and S. Selberherr, Quantum transport in ultra-scaled double-gate MOSFETs: A Wigner function based Monte-Carlo approach, *Solid-State Electronics*, vol. 49, pp. 1510-1515, 2005.

Sze et al., 1988 : S. M. Sze, VLSI Technology, second edition, *McGraw-Hill Book Company*, p. 332 and following, 1988.

Tang et al., 2003 : T. Tang and B. Wu, Quantum corrected Monte Carlo simulation of semiconductor devices using the effective conduction-band edge method, *Journal of Computational Electronics*, vol. 2, pp. 131-135, 2003.

Tsuchiya et al., 2003 : H. Tsuchiya, M. Horino and T. Miyoshi, Quantum Monte Carlo device simulation of nano-scaled SOI-MOSFETs, *Journal of Computational Electronics*, vol. 2, pp. 91-95, 2003.

IntechOpen

Applications of Monte Carlo Method in Science and Engineering
Edited by Prof. Shaul Mordechai

ISBN 978-953-307-691-1
Hard cover, 950 pages
Publisher InTech
Published online 28, February, 2011
Published in print edition February, 2011

In this book, Applications of Monte Carlo Method in Science and Engineering, we further expose the broad range of applications of Monte Carlo simulation in the fields of Quantum Physics, Statistical Physics, Reliability, Medical Physics, Polycrystalline Materials, Ising Model, Chemistry, Agriculture, Food Processing, X-ray Imaging, Electron Dynamics in Doped Semiconductors, Metallurgy, Remote Sensing and much more diverse topics. The book chapters included in this volume clearly reflect the current scientific importance of Monte Carlo techniques in various fields of research.

How to reference
In order to correctly reference this scholarly work, feel free to copy and paste the following:

Marie-Anne Jaud, Sylvain Barraud, Philippe Dollfus, Jérôme Saint-Martin, Arnaud Bournel and Hervé Jaouen (2011). A Pearson Effective Potential for Monte-Carlo Simulation of Quantum Confinement Effects in nMOSFETs, Applications of Monte Carlo Method in Science and Engineering, Prof. Shaul Mordechai (Ed.), ISBN: 978-953-307-691-1, InTech, Available from: http://www.intechopen.com/books/applications-of-monte-carlo-method-in-science-and-engineering/a-pearson-effective-potential-for-monte-carlo-simulation-of-quantum-confinement-effects-in-nmosfets

INTECH
open science | open minds

InTech Europe
University Campus STeP Ri
Slavka Krautzeka 83/A
51000 Rijeka, Croatia
Phone: +385 (51) 770 447
Fax: +385 (51) 686 166
www.intechopen.com

InTech China
Unit 405, Office Block, Hotel Equatorial Shanghai
No.65, Yan An Road (West), Shanghai, 200040, China
中国上海市延安西路65号上海国际贵都大饭店办公楼405单元
Phone: +86-21-62489820
Fax: +86-21-62489821

© 2011 The Author(s). Licensee IntechOpen. This chapter is distributed under the terms of the Creative Commons Attribution-NonCommercial-ShareAlike-3.0 License, which permits use, distribution and reproduction for non-commercial purposes, provided the original is properly cited and derivative works building on this content are distributed under the same license.